Journal of Theoretical Biology 272 (2011) 42–54

Contents lists available at ScienceDirect

Journal of Theoretical Biology

journal homepage: www.elsevier.com/locate/yjtbi

Co-existent activity patterns in inhibitory neuronal networks with short-term synaptic depression

Amitabha Bose [a,c,*], Victoria Booth [b]

[a] Department of Mathematical Sciences, New Jersey Institute of Technology, Newark, NJ 07102, USA
[b] Departments of Mathematics and Anesthesiology, University of Michigan, Ann Arbor, MI 48109, USA
[c] School of Physical Sciences, Jawaharlal Nehru University, New Delhi 110067, India

ARTICLE INFO

Article history:
Received 19 May 2010
Received in revised form
18 October 2010
Accepted 1 December 2010
Available online 9 December 2010

Keywords:
Dynamical systems
Periodic orbit
Synaptic depression

ABSTRACT

A network of two neurons mutually coupled through inhibitory synapses that display short-term synaptic depression is considered. We show that synaptic depression expands the number of possible activity patterns that the network can display and allows for co-existence of different patterns. Specifically, the network supports different types of n–m anti-phase firing patterns, where one neuron fires n spikes followed by the other neuron firing m spikes. When maximal synaptic conductances are identical, n–n anti-phase firing patterns are obtained and there are conductance intervals over which different pairs of these solutions co-exist. The multitude of n–m anti-phase patterns and their co-existence are not found when the synapses are non-depressing. Geometric singular perturbation methods for dynamical systems are applied to the original eight-dimensional model system to derive a set of one-dimensional conditions for the existence and co-existence of different anti-phase solutions. The generality and validity of these conditions are demonstrated through numerical simulations utilizing the Hodgkin–Huxley and Morris–Lecar neuronal models.

© 2010 Elsevier Ltd. All rights reserved.

1. Introduction

Short-term synaptic depression is widely found in synapses of the central nervous system (Abbott and Regehr, 2004) and in central pattern generating networks (O'Donovan et al., 1998; Rabbah and Nadim, 2007). Depressing synapses display changes in their strength as a function of firing frequency. In particular, when the activation frequency of a pre-synaptic cell is high, then its synapse depresses with each subsequent spike weakening its effect on a post-synaptic cell. Alternatively, when the activation frequency is low, the synapse recovers to a strong state between each spike and has a much larger effect on the post-synaptic cell. The effect of synaptic depression on network behavior depends, in some measure, on network structure, particularly whether a network is generally feedforward in design or includes feedback projections among its constituent neurons (see Grande and Spain, 2005 for a review). In reciprocally connected networks, depression has been shown to broaden network dynamics in a variety of ways, such as by generating rhythmic spontaneous activity (Rubin et al., 2009; Tabak et al., 2000), regulating the relative timing of firing of network components (Manor et al., 2003; Mouser et al., 2008), supporting persistent activity (Barbieri and Brunel, 2007) and introducing co-existing stable firing patterns (Bose et al., 2001; Chandrasekaran et al., 2009; Jalil et al., 2004; Manor and Nadim, 2001; Nadim et al., 1999). Understanding the contributions of synaptic depression to the generation of such diverse patterns of activity is often best achieved by studying small, idealized networks of model neurons. Indeed, the study of small minimal models (as small as two neurons) continues to reveal important insights into the operation of neuronal networks of any scale (Skinner et al., 2005). Despite their small size, minimal networks display remarkable complexity in their dynamic states.

In this study, we consider how synaptic depression can be utilized to create co-existence of different types of anti-phase solutions in a network of two mutually coupled inhibitory neurons. We show that, largely independent of the specific neuron model used, depression introduces a multitude of co-existent n–n anti-phase firing states. In an n–n firing pattern, neuron 1 fires n consecutive spikes followed by n consecutive spikes of neuron 2 and so on. As the maximal synaptic conductance is increased, the network can switch from 1–1 to 2–2 to 3–3 and higher anti-phase firing. We also find that there are ranges of the maximal synaptic conductance over which pairs of these solutions co-exist. Interestingly, when the synapses do not display synaptic depression, these intervals of co-existence largely disappear and the network supports a smaller number of different n–n firing patterns.

In the context of network bistability with depressing synapses, Nadim et al. (1999) introduced the concept of a cell-controlled

* Corresponding author at: Department of Mathematical Sciences, New Jersey Institute of Technology, Newark, NJ 07102, USA. Tel.: +1 973 596 3370; fax: +1 973 596 5591.
E-mail address: bose@njit.edu (A. Bose).

0022-5193/$ - see front matter © 2010 Elsevier Ltd. All rights reserved.
doi:10.1016/j.jtbi.2010.12.001

versus synapse-controlled network. In the former, the intrinsic dynamics of the individual neurons determine the network frequency, which is necessarily high so that the synapses can remain depressed and largely irrelevant. In the synapse-controlled case, the dynamics of the synapse determine the network frequency which is typically much lower than in the cell-controlled scenario. In this paper, we expand on this idea to show that there are several levels of synapse-controlled oscillations each of which corresponds to a different n–n anti-phase firing pattern. Each of these patterns is characterized by distinct levels of synaptic depression and recovery. The primary implication of this finding is therefore that the type of co-existence that we find is largely independent of the intrinsic dynamics of the neurons. As a result, different types of neuronal models should be able to exhibit co-existence simply by allowing the synapses between cells to display the appropriate level of synaptic depression. We illustrate the generality of this result through simulations using two different neuron models, the Hodgkin–Huxley model and the Morris–Lecar model. We have chosen parameters such that the models operate in very different frequency regimes and show how the ensuing network dynamics can be understood through an analysis of the synapses between neurons that largely ignores the intrinsic dynamics of these neurons.

A primary goal of this paper is not just to show co-existence of solutions, but also to describe a methodology by which properties of these solutions can be understood. To that end, we use a combination of numerical simulations and analysis. In particular, simulations of different neuron models are used to show co-existence of various n–n solutions. Rather than rigorously proving the existence and stability of these solutions, we use analytic methods to extract the key reasons why these solutions should exist. One advantage of this approach is that it allows us to isolate the mechanisms that underlie the existence of these solutions and the transitions between them without becoming too deeply ensnared in the mathematical content. The main mathematical tool to conduct the analysis is geometric singular perturbation theory which is used to derive reduced sets of equations that govern the behavior of solutions along different parts of the trajectory. We focus on deriving necessary and sufficient conditions for the existence and co-existence of solutions. In particular, we are able to collapse the 8-dimensional network model to the study of two distinct 1-dimensional objects to establish these conditions. One of the aims of the paper is to show that in certain circumstances, as described in the text, identifying the correct lower-dimensional quantity of interest is as valuable as actually proving the existence of the solution.

The paper is organized as follows. In Section 2, we introduce our minimal network model with depressing synapses and describe the reduced equations that govern solutions along different parts of the trajectory. Section 3 contains the main results, which begin with numerical simulations of the network utilizing the Hodgkin–Huxley and Morris–Lecar equations. We then analytically derive conditions for the existence and co-existence of different n–n anti-phase solutions when the synapses between cells are identical. We also consider the case when synaptic strengths are heterogeneous which gives rise to more complicated n–m (e.g. 2–1, 3–1, 3–2 etc.) anti-phase firing patterns and illustrate how to derive conditions for their existence. Section 4 contains a discussion.

2. Model

We consider two different well-known models of neuronal activity, the Hodgkin–Huxley and the Morris–Lecar models. The Hodgkin–Huxley model (Hodgkin and Huxley, 1952) is a set of four first order equations that describe the kinetics of sodium, potassium and leak currents that generate action potential firing. The Morris–Lecar model (Morris and Lecar, 1981) is a set of two first order equations in which calcium, potassium and leak currents contribute to firing solutions. See Appendix for specific equations and parameter values.

The mathematical analysis is performed on a generic relaxation oscillator model whose basic dynamics replicate the tonic spiking behavior of either of the models that we simulate. We first consider the case when both neurons are identical, intrinsic oscillators with identical synapses. Equations for each neuron can be written as

$$\varepsilon v_i' = f(v_i,w_i) - \overline{g} s_j [v_i - E_{inh}],$$

$$w_i' = h(v_i,w_i),$$

$$d_i' = \begin{cases} (1-d_i)/\tau_a & \text{if } v_i < v_\theta, \\ -d_i/\tau_b & \text{if } v_i > v_\theta, \end{cases}$$

$$s_i' = \begin{cases} -s_i/\tau_k & \text{if } v_i < v_\theta, \\ 0 & \text{if } v_i > v_\theta, \end{cases} \tag{1}$$

where $i, j = 1, 2$. The function $f(v,w)$ incorporates the ionic currents intrinsic to each cell, $h(v,w)$ models the gating of one of the currents, s_j is the synaptic gating variable governing the input from neuron j to neuron i, and v_θ is the synaptic threshold. The parameters $\overline{g}$ and E_{inh} are the maximal conductance and reversal potential of the synapse, respectively. As modeled in Bose et al. (2001), the variable d_i is a depression variable which tracks the extent of depression and recovery of the synapse from cell i to cell j and depends on the amount of time a neuron spends above and below threshold. The synaptic gating variable s_i and the depression variable d_i are linked through the following reset condition: whenever the voltage of neuron i increases above the synaptic threshold v_θ, s_i is instantaneously reset to the current value of d_i. More specifically, if a presynaptic action potential occurs at $t=0$, then we reset $s_i(0^+)$ to equal $d_i(0)$. At all other times, except the moment when the presynaptic neuron increases above threshold, d_i and s_i are uncoupled and obey Eqs. (1). This discontinuous reset is consistent with other phenomenological models of synaptic depression (Abbott et al., 1997; Tsodyks and Markram, 1997). To model a non-depressing synapse, we replace the d_i' equation with $d_i \equiv 1$. In the non-depressing case, the synaptic variable s_i is always reset to the value 1 and thus synaptic strength does not depend on the time the presynaptic neuron spends above and below threshold.

We assume that the set of points satisfying $f(v,w)=0$ forms a cubic-shaped nullcline curve and the set satisfying $h(v,w)=0$ forms a sigmoidal-shaped nullcline curve in the v–w phase plane (Fig. 1). When $\overline{g} = 0$ and the cells are uncoupled, we choose parameters so

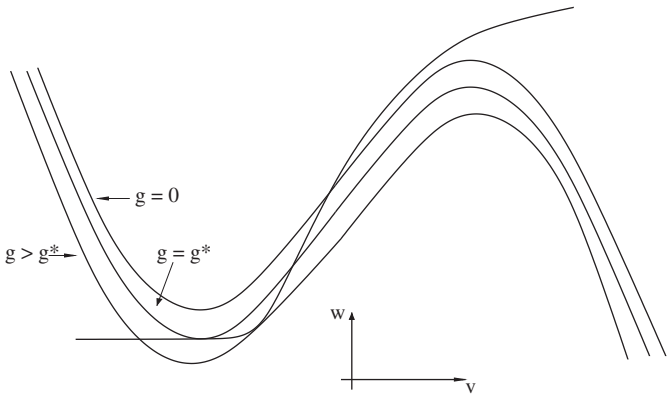

Fig. 1. Nullcline curves $f(v_i, w_i)=0$ (cubic-shaped v-nullcline) and $h(v_i, w_i)=0$ (sigmoidal-shaped w-nullcline) in the v–w phase plane for different values of the synaptic conductance $g = \overline{g}s$. Larger values of g shift the v-nullcline downward causing the location of the fixed point to move from the middle to the left branch. The v- and w-nullclines intersect tangentially when $g = g^*$.

that the intersection of these two curves occurs along the middle branch of the cubic. The ensuing fixed point is unstable and there exists a periodic solution that encloses it. We shall assume that the period of this orbit is given by $T = T_{act} + T_{inact}$, where T_{act} is the amount of time the orbit spends in the active state defined by $v > v_\theta$ and T_{inact} is the amount of time spent in the silent state when $v < v_\theta$. When $\overline{g} > 0$, the cubic v-nullcline shifts down in the v-w phase plane and the intersection point with the w-nullcline moves. If the product $g = \overline{g}s$ is sufficiently large, then the intersection point will occur on the left branch of the shifted v-nullcline and the fixed point will be stable (Fig. 1). Let $F(v,w,g) = f(v,w) - g[v - E_{inh}]$. There exists a unique value $g^\star$ such that $F(v,w,g^\star) = 0$ and $\partial F/\partial v(v,w,g^\star) = \partial h/\partial v(v,w,g^\star)$. This is the value at which the v- and w-nullclines share a tangency at their intersection. Thus for any $g > g^\star$ the intersection will occur on the left branch. Note for sufficiently large $\overline{g}$, there exists a unique value $s^\star \in (0,1)$ such that $g^\star = \overline{g}s^\star$.

In the limit $\varepsilon \to 0$, (1) becomes a singularly perturbed set of equations allowing us to define fast and slow timescale separations. First, by rescaling $t = \varepsilon\xi$ and then letting $\varepsilon = 0$, we obtain the fast equations (derivative with respect to ξ)

$$\begin{aligned} \dot{v}_i &= f(v_i,w_i) - \overline{g}s_j[v_i - E_{inh}], \\ \dot{w}_i &= 0, \\ \dot{d}_i &= 0, \\ \dot{s}_i &= 0. \end{aligned} \tag{2}$$

These equations govern the fast transitions between the left and right branches of the v-nullcline. When $\varepsilon = 0$ in (1), we obtain the slow equations (derivative with respect to t)

$$\begin{aligned} 0 &= f(v_i,w_i) - \overline{g}s_j[v_i - E_{inh}], \\ w_i' &= h(v_i,w_i), \\ d_i' &= \begin{cases} (1-d_i)/\tau_a & \text{if } v_i < v_\theta, \\ -d_i/\tau_b & \text{if } v_i > v_\theta, \end{cases} \\ s_i' &= \begin{cases} -s_i/\tau_k & \text{if } v_i < v_\theta, \\ 0 & \text{if } v_i > v_\theta. \end{cases} \end{aligned} \tag{3}$$

The first of these equations restricts the solution flow to the v-nullcline while the remaining three equations govern the dynamics of the flow on that nullcline. We further assume that $\partial F/\partial v \neq 0$ at all points of the v-nullcline except for the local minimum and maximum points. This allows us to use the implicit function theorem to solve for v in the first equation of (3) in terms of w and s and substitute into the others. Solutions from the fast and slow equations are then pieced together to find a singular periodic orbit that is valid when $\varepsilon = 0$ (Fig. 2). It is well established how to extend this solution for ε sufficiently small to find an actual periodic orbit that lies in a neighborhood of the singular orbit; see Mishchenko and Rozov (1980) for example.

For the analysis presented here, we shall concentrate on the slow equations when a neuron is in its silent state ($v_i < v_\theta$). In this case, we require one new definition and one assumption. First, in an n–n solution, one cell spikes n times while the other cell remains silent, followed by n spikes of the latter cell while the former is silent. In this situation, the spiking cell in each cycle has moments of being active and of being silent. We shall say that during these times, the cell is "free". The cell that remains below threshold and is always silent during this time will be called "quiet". The assumption that we make is that when a cell is free, spiking occurs with the uncoupled period $T = T_{act} + T_{inact}$. As will be seen in the results section, both the Hodgkin–Huxley and Morris–Lecar models satisfy this assumption. Further, it is a natural assumption since the inhibition to the free cell is constantly decaying, implying that eventually the free cell will spike with its uncoupled period. This assumption allows us to easily keep track of the free cell's dynamics and to concentrate on the behavior of the quiet cell to determine when it eventually leaves the silent state.

To determine when a quiet cell can fire, first consider the case that the w-nullcline has zero slope near the left branch of the v-nullcline. Then a necessary condition for the quiet cell to be able to fire is $\overline{g}s < g^\star$. If the w-nullcline has non-zero slope, this necessary condition still holds provided that the attraction to the w-nullcline is sufficiently strong. This latter condition is satisfied when the rate of decay in the w direction is much faster compared to the rate in the s direction (w' much greater than s'). When it holds, the necessary condition $\overline{g}s < g^\star$ also becomes sufficient for the quiet cell to fire. In short, it implies that when the fixed point on the left branch of the quiet cell's v nullcline disappears, the quiet cell fires.

The conditions for firing just described allow us to keep track of the depression and synaptic variables of the free cell, and relate their values to the existence of different types of equations. Further, since s_i is reset to d_i at every instance when the free cell goes above threshold, we need only keep track of the depression variables from cycle to cycle. In this way, the potentially complicated dynamics of

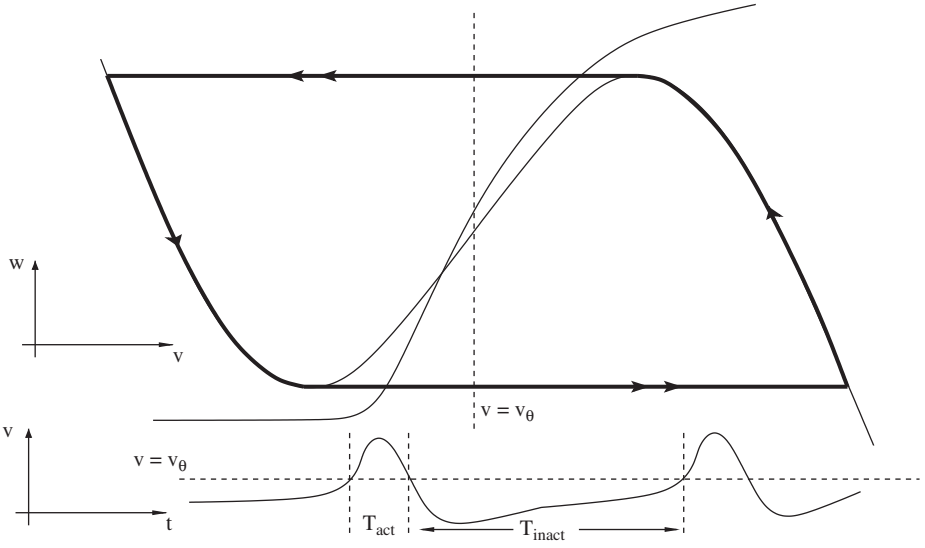

Fig. 2. Intrinsic oscillatory solution of a model neuron. In the top panel, the singular, intrinsic periodic orbit is shown in the v–w phase plane. Double (single) arrows indicate solutions of the fast (slow) equations. The lower panel shows a v vs. t graph of the intrinsic orbit and demarcates the times T_{inact} and T_{act}.

the eight-dimensional system (1) can be reduced to studying relatively simple one-dimensional quantities.

In the section below, we shall refer to solutions that are numerically stable. These are solutions that we found through simulation, and numerically, attract nearby initial conditions. We do not analytically prove this stability, but instead derive conditions concerning the existence and co-existence of these solutions. This approach balances the need to intuitively understand the existence of certain solutions versus the potential quagmire of getting too deeply engrossed in mathematical detail. The approach is also, in part, complementary to the more familiar method of proving existence of solutions by finding fixed points of reduced maps. In the discussion section, we will elaborate on this last point.

3. Results

First, we present numerical simulations of two-cell inhibitory networks that demonstrate the existence and co-existence of different anti-phase firing patterns using the Hodgkin–Huxley and Morris–Lecar models. These results indicate that the interesting dynamics of the network have less to do with the intrinsic properties of the cells and more to do with the synapses between them. In turn, this allows us to focus our analysis on the behavior of the synapses to understand why these solutions arise.

3.1. Simulations of mutually inhibitory networks

In two-cell, mutually inhibitory networks when synapses are non-depressing, several different anti-phase firing patterns can be obtained as the maximum synaptic conductance is varied. For example, for networks of Hodgkin–Huxley or Morris–Lecar model neurons under the parameter regimes we consider (see Appendix for equations and parameter values), when synaptic conductances are homogeneous and weak ($\bar{g} \leq 10.7$ mS/cm^2 for the Hodgkin–Huxley network; $\bar{g} \leq 0.173$ mS/cm^2 for the Morris–Lecar network), the two neurons alternately fire single spikes in a classic 1–1 anti-phase pattern. As maximum synaptic conductances are increased identically ($11.2 \leq \bar{g} < 12.9$ mS/cm^2 for the Hodgkin–Huxley network; $0.175 \leq \bar{g} < 0.179$ mS/cm^2 for the Morris–Lecar network), a 2–2 anti-phase pattern becomes numerically stable where the neurons alternately fire two spikes each. In the $\bar{g}$ interval between numerically stable 1–1 and 2–2 firing, inconsistent, alternating 1–1, 2–1 and 2–2 firing occurs. For larger values of $\bar{g}$ ($\bar{g} \geq 13.0$ mS/cm^2 for the Hodgkin–Huxley network; $\bar{g} \geq 0.179$ mS/cm^2 for the Morris–Lecar network), one cell is able to completely suppress the firing of the other cell. Either cell is capable of being suppressed by the other, hence these symmetric modes are numerically bistable for large values of the maximum synaptic conductance.

When the synapses in either the Hodgkin–Huxley or Morris–Lecar networks are depressing, more anti-phase firing patterns can be obtained over different ranges of maximum synaptic conductance values. As in the non-depressing case, for smaller values of $\bar{g}$, 1–1 anti-phase firing is obtained (see Table 1 for $\bar{g}$ values). As $\bar{g}$ is increased, 1–1 anti-phase gives over to 2–2 anti-phase but now there are small ranges of $\bar{g}$ values where either mode can be obtained and numerical bistability has been introduced. Specifically, the maximum $\bar{g}$ value where 1–1 anti-phase firing is numerically stable is less than the minimum $\bar{g}$ value where 2–2 anti-phase firing is numerically stable (Table 1). As shown in Fig. 3A and in Fig. 4A, both the Hodgkin–Huxley and Morris–Lecar networks can be switched between the 1–1 anti-phase mode and the 2–2 anti-phase mode when $\bar{g}$ is fixed in this interval. In both networks, the switch is induced by reducing the applied current to each cell, indicated by the heavy black bar above the top trace in both figures. In the cases shown, during this reduction of applied current, firing is suppressed or firing frequency of one cell is decreased allowing the other cell to spike twice (1st and 3rd traces in the figures). In either case, the switch requires that the synapse of the quiet cell is able to sufficiently recover such that, when it spikes again, inhibition to the other cell is increased from the levels in the 1–1 solution. With increased inhibition, as evidenced by the higher maximum values of d_i and s_i (2nd and 4th traces in the figures), the now quiet cell is unable to fire before the free cell fires a second spike, thus leading to a 2–2 anti-phase pattern.

For larger values of $\bar{g}$, additional anti-phase patterns are obtained with small regions of numerical bistability near the synaptic conductance values where the modes transition. For both networks, 3–3 anti-phase firing is obtained in the $\bar{g}$ intervals given in Table 1 and there is numerical bistability in the $\bar{g}$ intervals between the maximum value where 2–2 firing is numerically stable and the minimum value where 3–3 firing is numerically stable. This numerical bistability between 2–2 firing and 3–3 firing is shown in Figs. 3B and 4B where the switch between modes is induced in the same way as in part A of the figures. Again note that the maximum values of d_i and s_i are larger in the 3–3 solution than for the 2–2 pattern (2nd and 4th traces).

These similar n–n firing patterns and $\bar{g}$ intervals of numerical bistability between anti-phase modes occurs in these two networks regardless of differences in neuronal properties, such as shape and width of action potentials or the $\approx$ 20-fold difference in the intrinsic periods T of the model neurons ($T \approx 17$ ms in the Hodgkin–Huxley model and $T \approx 376$ ms in the Morris–Lecar model). For all the n–n firing solutions, periods of the cycling patterns increase with increasing $\bar{g}$. Additionally, at the terminal values of $\bar{g}$ where the n–n patterns lose numerical stability, we observe that periods in both networks relate to the intrinsic periods of the constituent neurons. Namely, 1–1 firing loses numerical stability when its period equals $2T$, twice the intrinsic cell period; 2–2 firing loses numerical stability at a period of $4T$ and numerically stable 3–3 anti-phase firing terminates at a period of $6T$. Within the burst of spikes of the n–n solutions at the terminal value of $\bar{g}$, the inter-spike interval is basically equal to the intrinsic period of the uncoupled cell, as can be

Table 1
Properties of n–n (for $n=1,2,3$) anti-phase solutions in two-cell mutually inhibitory networks of Hodgkin–Huxley and Morris–Lecar model neurons including period of intrinsic oscillations in each model neuron (T), maximal synaptic conductance $\bar{g}$ values for which n–n solutions are numerically stable, period of n–n oscillation at the maximum $\bar{g}$ value where the n–n solution loses numerical stability, and duration of inter-spike intervals (ISIs) between successive spikes of an individual cell. For weakest synaptic conductances in the Hodgkin–Huxley network ($\bar{g}$ values less than 0.1 mS/cm^2), cells are virtually uncoupled and observed solutions sensitively depend on initial conditions.

	n–n solution	$\bar{g}$ values (mS/cm^2)	Period (ms) at terminal $\bar{g}$	ISI(s) (ms) at terminal $\bar{g}$
Hodgkin–Huxley	1–1	0.1–20.60	34.3 ($\sim 2T$)	–
($T = 17.15$ ms)	2–2	20.28–25.63	68.7 ($\sim 4T$)	17.3 ($\sim T$)
	3–3	24.82–26.186	102.8 ($\sim 6T$)	17.0, 17.2 ($\sim T$)
Morris–Lecar	1–1	0–0.388	751.1 ($\sim 2T$)	-
($T = 376.3$ ms)	2–2	0.370–0.467	1504.1 ($\sim 4T$)	376.6 ($\sim T$)
	3–3	0.456–0.515	2256.7 ($\sim 6T$)	376.6, 376.3 ($\sim T$)

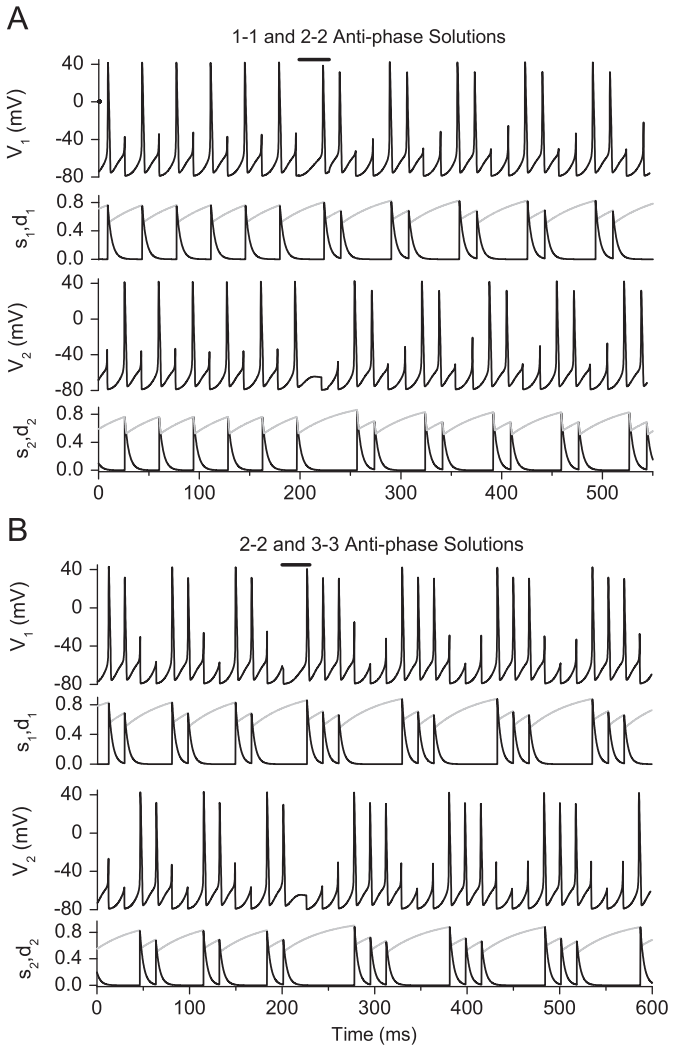

Fig. 3. Co-existence between n–n anti-phase solutions in a two-cell mutually inhibitory network of Hodgkin–Huxley model neurons. Numerically stable 1–1 anti-phase firing is switched to a numerically stable 2–2 anti-phase firing with maximal synaptic conductance fixed at $\overline{g} = 20.4$ mS/cm^2 (A) and a numerically stable 2–2 anti-phase firing is switched to a numerically stable 3–3 anti-phase firing with $\overline{g} = 25$ mS/cm^2 (B). A and B: Voltage traces for Cell 1 (top panel) and Cell 2 (3rd panel) show cells initially in a 2-2 anti-phase firing pattern. A transient, hyperpolarizing current pulse (heavy bar) applied to both cells switches the solution to a 3-3 anti-phase firing pattern. Depression variable d_1 (gray curves) and synaptic variable s_1 (black curves) from cell 1 to cell 2 (2nd panel) and d_2, s_2 from cell 2 to cell 1 (bottom panel) reach larger maximum values in the 3-3 antiphase pattern indicating a greater recovery from depression on each cycle and thus a stronger synapse.

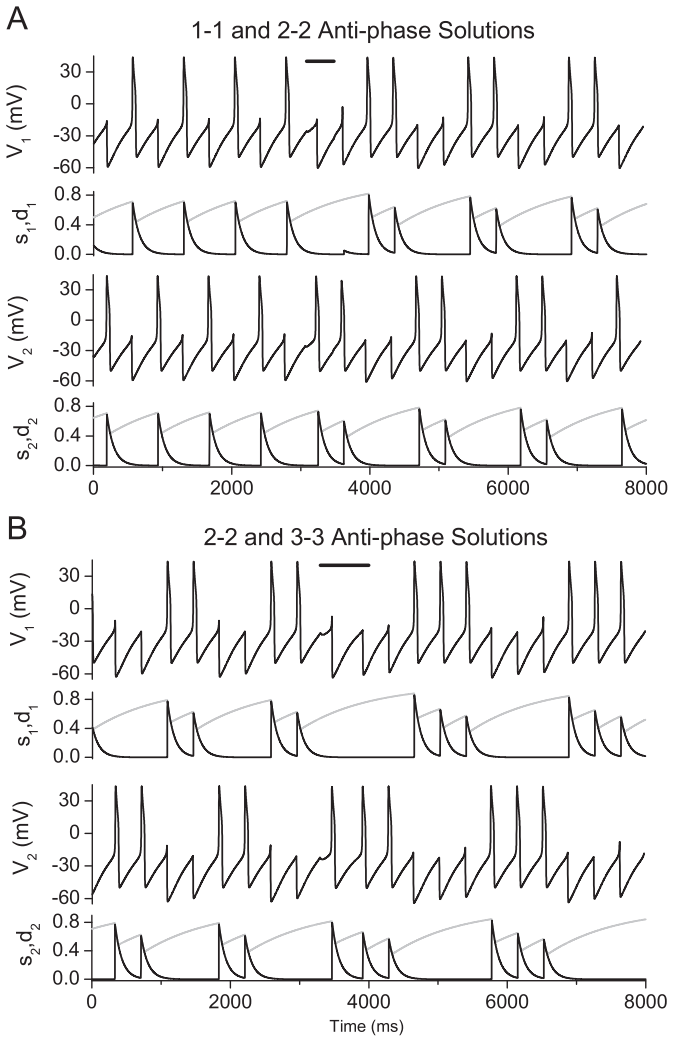

Fig. 4. Co-existence between n–n anti-phase solutions in a two-cell mutually inhibitory network of Morris–Lecar model neurons. Numerically stable 1–1 anti-phase firing is switched to a numerically stable 2–2 anti-phase firing with maximal synaptic conductance fixed at $\overline{g} = 0.38$ mS/cm^2 (A) and a numerically stable 2–2 anti-phase firing is switched to a numerically stable 3–3 anti-phase firing with $\overline{g} = 0.46$ mS/cm^2 (B). A and B: Traces in panels same as in (Fig. 3).

expected since the free cell is not receiving any input from the quiet cell. Later in Section 3.4, we will analytically explain why the bifurcation from a n–n solution occurs at periods of $2nT$.

In both networks, numerically stable higher value n–n anti-phase firing patterns are obtained in increasingly smaller intervals of $\overline{g}$ as it is increased. For the Morris–Lecar network, we have numerically computed a bifurcation diagram plotting the periods of different n–n solutions that exist over a range of $\overline{g}$ values (Fig. 5). Numerically stable solution branches (solid curves) for n–n ($n=1$–5) anti-phase firing patterns are plotted over the $\overline{g}$ intervals in which they exist. For the highest $\overline{g}$ values, one cell can completely suppress firing in the other cell and, as in the non-depressing synapse case, there is numerical bistability of these symmetric cell suppressed solutions. In the $\overline{g}$ interval between numerically stable 5–5 anti-phase firing and the cell suppressed solutions, numerically stable 6–6, 7–7 and 8–8 anti-phase firing occurs. For all n–n solutions, the period is an increasing function of $\overline{g}$, although the period does not vary significantly for the higher n–n patterns. Moreover as $\overline{g}$ increases, each n–n solution loses numerical stability when the period is equal to $2nT$. The dotted vertical drop lines at the beginning and termination of each stable branch indicate the regions of co-existence of different n–n firing patterns. There is a very small $\overline{g}$ interval in which 3–3 and 4–4 anti-phase solutions are both numerically stable, but in the $\overline{g}$ intervals between numerically stable higher n–n firing solutions, unsymmetric and inconsistent $m-n$ anti-phase firing patterns appear. Solutions of the Hodgkin–Huxley network follow similar trends for higher $\overline{g}$ values. The following sections are dedicated to providing an analytic explanation for these simulation results.

The solution branches for 1–1, 2–2, 3–3 anti-phase firing and cell suppressed firing were computed with numerical continuation software (see Appendix) that was able to follow the solutions around the limit points where numerical stability was lost and identify numerically unstable solution branches (gray dashed curves). For 1–1, 2–2 and 3–3 anti-phase firing, these unstable solutions form isolas connecting the ends of the stable branch at low and high $\overline{g}$ values. While full analysis of these numerically unstable solutions is beyond the focus of this paper, we note that these solutions consist of n–n anti-phase firing with variable spike

amplitudes. Since periodic solutions in the Morris–Lecar model occur via a subcritical Hopf bifurcation in the parameter range we consider, it may be that these numerically unstable solutions involve the unstable periodic solutions associated with that bifurcation.

3.2. Conditions for n–n firing patterns

We now turn to deriving conditions for the existence of the observed n–n solutions. In these solutions, at any moment in time, exactly one of the cells is free, while the other is quiet. The free cell fires with its intrinsic period T. After n firings of the free cell, it becomes quiet, and the previously quiet cell becomes free and begins firing. We will determine conditions for how many times the free cell fires before becoming quiet and also determine the times at which these switches occur.

Let us first discuss 1–1 anti-phase periodic solutions. For the sake of argument, assume that cell one fires every $2nT$, while cell 2 fires every $(2n-1)T$. Thus we are assuming that one of the two cells fires every nT. This condition simplifies the situation allowing us to show why co-existence can occur. Later we will relax this assumption. The first point to note is that due to the separation of time scales, the coupling of s to d at the moment of a spike and the assumption that a quiet cell in the silent state is strongly attracted toward the w-nullcline, the relevant quantity to consider is the value of d at the moment a cell jumps to the active state. Suppose at $t=0$, cell 1 becomes free and jumps to the active state with an initial value of d_1 given by $d_1(0)$. Cell 1 returns to the silent state at $t=T_{act}$ with $d_1(T_{act}) = d_1(0)\exp(-T_{act}/\tau_b)$. At $t=T$, cell 2 becomes free and jumps to the active state staying there until $t=T+T_{act}$. Then at $t=2T$, cell 1 is ready to become free again. During the time $t \in (T_{act}, 2T)$, d_1 increases according to $d_1' = (1-d_1)/\tau_a$. Thus at $t=2T$,

$$d_1(2T) = 1-(1-d_1(T_{act}))e^{-(T+T_{inact})/\tau_a}.$$

A necessary condition for a 1–1 periodic solution is that $d_1(0)=d_1(2T)$. Substituting for $d_1(2T)$ and $d_1(T_{act})$, solving for $d_1(0)$ and denoting this new value by d_{1-1}, we obtain

$$d_{1-1} = \frac{1-e^{-(T+T_{inact})/\tau_a}}{1-e^{-T_{act}/\tau_b}e^{-(T+T_{inact})/\tau_a}}. \tag{4}$$

It is easy to see that d_{1-1} is actually the maximum value that $d_1(t)$ (and $d_2(t)$) takes along the periodic solution. It is also the value that s_i is reset to whenever a cell jumps to the active state. This observation leads directly to a useful version of the necessary condition for 1–1 firing. Note that $s_1(0)=d_{1-1}$ and since $s'_1 = 0$ when cell 1 is active, $s_1(T) = d_{1-1}\exp(-T_{inact}/\tau_k)$. Using the necessary condition for a cell to fire, $\bar{g}s(t) < g^\star$, we find after substitution and rearrangement

$$\bar{g}d_{1-1}e^{-T_{inact}/\tau_k} < g^\star. \tag{5}$$

This condition guarantees that the free cell spikes no more than once before the quiet cell reaches threshold. Eq. (5) is instructive in many ways. First if we consider $g^\star$, T_{inact}, T_{act} and τ_k to be fixed, it provides an upper bound on the maximal synaptic conductance for the 1–1 solution to exist in terms of the depression and recovery time constants. Thus the condition relates how the different aspects of the synapse regulate the existence of the 1–1 firing pattern. For example, if the synapse recovers very quickly from depression $\tau_a \to 0$, then $d_{1-1} \to 1$, and the synapse acts more like a non-depressing one. Further (5) becomes more difficult to satisfy as the left-hand side becomes larger. Similarly, increasing the synaptic conductance $\bar{g}$ makes the left-hand side of (5) larger, again making it harder to satisfy (Fig. 6). In both of these

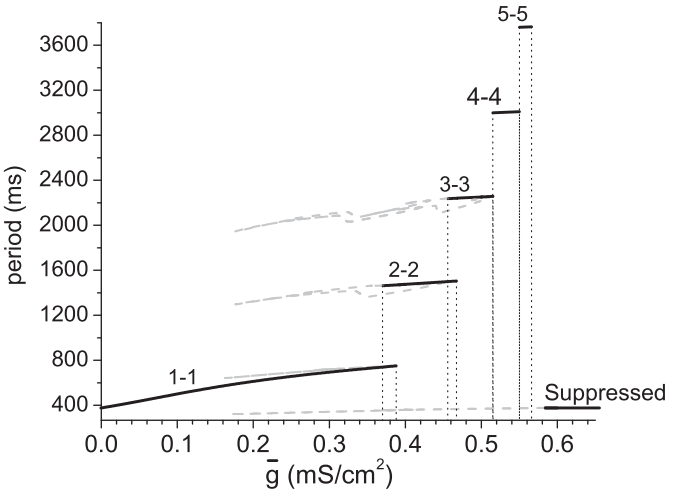

Fig. 5. Bifurcation diagram of numerically stable n–n antiphase solutions (solid curves) in the two-cell mutually inhibitory network of Morris–Lecar model neurons as $\bar{g}$ is increased from 0 to 0.65 mS/cm^2. Intervals of $\bar{g}$ where co-existence occurs between successive n–n solutions are indicated by overlap of the dotted vertical drop lines at the initial and terminal $\bar{g}$ values where each n–n solution is numerically stable. In the $\bar{g}$ interval between the numerically stable 5–5 solution and the cell suppressed solutions, higher n–n numerically stable solutions exist in very narrow ranges of $\bar{g}$. Branches of unstable periodic solutions extend from some of the numerically stable n–n solutions and form isolas (gray dashed curves).

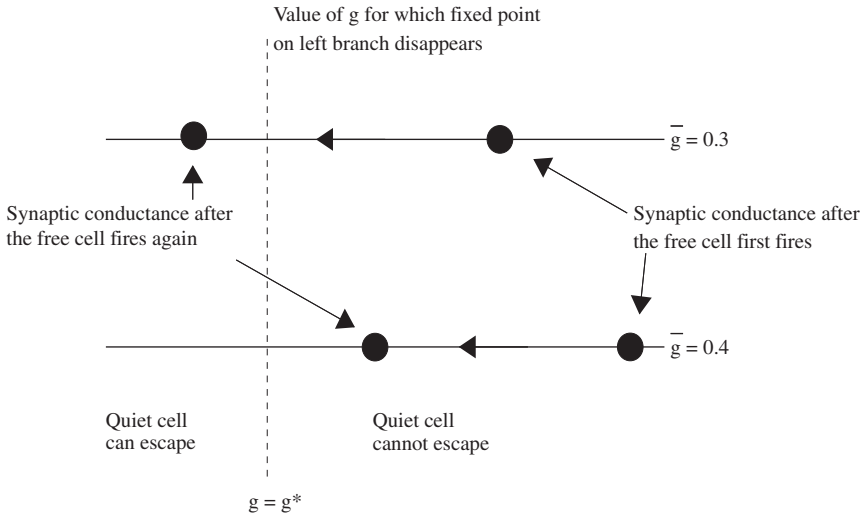

Fig. 6. The g phase line. Two different values of $\bar{g}$ are shown. For both, the region for which escape is possible is marked. In the top panel, since $\bar{g}$ is small, the conductance drops below $g^\star$ after one cycle while in the lower panel with larger $\bar{g}$, it does not. 1–1 firing is possible in the first case, but not the second.

scenarios, there is a net increase in inhibition thus pushing the network away from the 1–1 firing pattern. The opposite is true when $\tau_b \to 0$ and the synapse depresses very quickly. In this scenario, 1–1 firing is more likely to occur. When $\tau_k \to 0$, the left-hand side of (5) tends to 0 and the condition is always satisfied. In this case, the two cells are effectively uncoupled.

If (5) is not satisfied, when for example, $\bar{g}$ is too large, then a suppressed solution can occur. In this situation, for all time, the free cell remains free, while the quiet cell remains suppressed. To derive a sufficient condition for when suppression occurs, suppose cell 1 fires periodically (period $=T$). Let $t=0$ denote the moment that cell 1 becomes active with initial d_1 value of d_s. Then by periodicity $d_1(T)=d_s$ which can be found using (3):

$$d_s = \frac{1-e^{-T_{inact}/\tau_a}}{1-e^{-T_{act}/\tau_b}e^{-T_{inact}/\tau_a}}. \tag{6}$$

In order for cell 1 to suppress the activity of cell 2, $\bar{g}s_1(T^-) > g^\star$, where $s_1(T^-) = d_s \exp(-T_{inact}/\tau_k)$. This leads to a sufficient condition for suppression to occur

$$\bar{g}d_s e^{-T_{inact}/\tau_k} > g^\star. \tag{7}$$

Note that as $\bar{g}$ increases, the left-hand side of (7) increases making the equation easier to satisfy. We will show below that 1–1 and suppressed firing cannot co-exist, thus suggesting that when (5) is not satisfied, other types of solutions should exist.

One such solution is a 2–2 firing pattern. To find this solution, use periodicity to solve $d_1(0)=d_1(4T)$. Denoting this common value by d_{2-2}, after some basic, but tedious calculations, we find

$$d_{2-2} = \frac{1-(1-(1-e^{-T_{inact}/\tau_a})e^{-T_{act}/\tau_b})e^{-(2T+T_{inact})/\tau_a}}{1-e^{-2T_{act}/\tau_b}e^{-(2T+2T_{inact})/\tau_a}}. \tag{8}$$

In order to guarantee that the free cell spikes at least two times prior to becoming quiet, $\bar{g}s_1(T^-) = \bar{g}d_{2-2}\exp(-T_{inact}/\tau_k) > g^\star$. Alternatively, to guarantee that the free cell spikes no more than two times, $\bar{g}s_1(2T^-) < g^\star$. Note that $s_1(2T^-) = s_1(T^+)\exp(-T_{inact}/\tau_k)$ where $s_1(T^+) = d_1(T)$ and $d_1(T)$ can be found by using (1) with $d_1(0)=d_{2-2}$. Doing so provides the following condition for 2–2 firing

$$\bar{g}[1-(1-d_{2-2}e^{-T_{act}/\tau_b})e^{-T_{inact}/\tau_a}]e^{-T_{inact}/\tau_k} < g^\star < \bar{g}d_{2-2}e^{-T_{inact}/\tau_k}. \tag{9}$$

The parameter dependencies associated with this condition are similar to those associated with (5). In particular, both the left and right sides of (9) are increasing functions of d_{2-2}. Thus changes in parameters that effect d_{2-2} would tend to shift the interval of $\bar{g}$ values over which the 2–2 solution exists rather than simply changing one end point of this interval.

To find general conditions on when an n–n solution can exist, we follow the same procedure as above to find the maximum value of d_{n-n} along an n–n periodic solution. Enforcing the periodicity condition $d_1(0)=d_1(2nT)$, we find

$$d_{n-n} = \frac{1-(1-(1-e^{-T_{inact}/\tau_a})\sum_{k=1}^{n-1} e^{-kT_{act}/\tau_b}e^{-(k-1)T_{inact}/\tau_a})e^{-(nT+T_{inact})/\tau_a}}{1-e^{-nT_{act}/\tau_b}e^{-n(T+T_{inact})/\tau_a}}. \tag{10}$$

We next observe that a condition for n–n firing is

$$\bar{g}d(nT^-)e^{-T_{inact}/\tau_k} < g^\star < \bar{g}d((n-1)T^-)e^{-T_{inact}/\tau_k}, \tag{11}$$

where the values $d((n\text{-}1)T^-)$ and $d(nT^-)$ depend on d_{n-n} and can be calculated using (3). Note that as $\bar{g} \to \infty$, (11) cannot be satisfied. In this limit, the condition (7) for suppression of one cell by the other holds. Thus for a fixed set of parameters (11) can be used to estimate the maximum value of n for which an n–n solution exists.

3.3. Co-existence and switching between different n–n firing patterns

Having derived conditions for the existence of n–n firing patterns, we now show that there are intervals of $\bar{g}$ values over which two different firing patterns can co-exist. Eqs. (5) and (9) provide upper and lower bounds on $\bar{g}$ for which 1–1 and 2–2 anti-phase solutions co-exist. Thus if

$$\bar{g}d_{1-1}e^{-T_{inact}/\tau_k} < g^\star < \bar{g}d_{2-2}e^{-T_{inact}/\tau_k} \tag{12}$$

both a 1–1 and a 2–2 solution can co-exist. For this equation to be satisfied, it is clear that d_{1-1} must be less than d_{2-2}. This is clearly seen in Figs. 3 and 4 which shows d vs. t traces for both the 1–1 and 2–2 solutions. We also numerically solved for d_{n-n} given by Eq. (10) for fixed values of T_{act} with different values of T_{inact} and n (Fig. 7). It is clearly seen that for any value of T_{inact}, $d_s < d_{1-1} < d_{2-2} < d_{3--3}$.

The necessary condition for the co-existence of an n–n and $(n+1)-(n+1)$ solution can be written simply as

$$\bar{g}d_{(n)}((n-1)T)e^{-T_{inact}/\tau_k} < g^\star < \bar{g}d_{(n+1)}((n-1)T)e^{-T_{inact}/\tau_k}, \tag{13}$$

where the notation $d_{(n)}$ refers to the value obtained over the $n-n$ solution by solving (3) with $d(0)=d_{n-n}$, while $d_{(n+1)}$ is solved on the $(n+1)-(n+1)$ solution with $d(0)=d_{n+1-n+1}$. The suppressed solutions may co-exist with an n–n solution if n is sufficiently large.

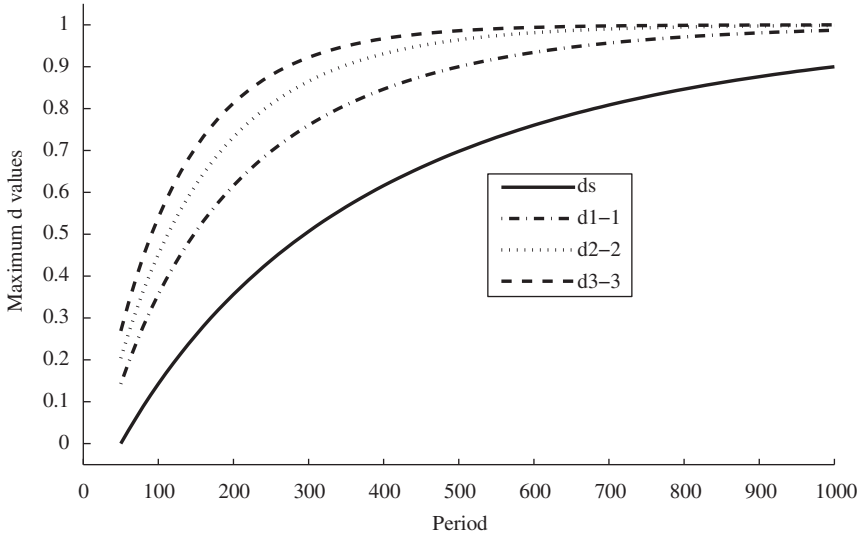

Fig. 7. Maximum d values along solutions obtained by numerically solving Eq. (10). The period was changed by increasing T_{inact} while keeping T_{act} constant. For any fixed value of the period, the values $d_{3-3} > d_{2-2} > d_{1-1} > d_s$. The following parameters were used: $T_{act}=50$, $\tau_b = 50$, $\tau_a = 500$.

The necessary condition for this case is

$$\overline{g}d_{(n)}((n-1)T)e^{-T_{inact}/\tau_k} < g^\star < \overline{g}d_s e^{-T_{inact}/\tau_k}. \quad (14)$$

Note that in the case that $n=1$, satisfaction of this condition would require $d_{1-1} < d_s$. However, as seen in Fig. 7, and as can be analytically shown, $d_s < d_{1-1}$, so a 1–1 and suppressed solution can never co-exist. That is why we say that n must be sufficiently large for co-existence of this type.

3.4. Relaxing the assumption of firing every nT

Having now gained an understanding of why co-existent firing patterns of different types should exist, let us remove the assumption that one of the two cells fires every nT. The main effect is that now the values d_{n-n} cannot be explicitly calculated. In fact the value of d_{n-n} will depend on $\overline{g}$ and the size of a particular interspike interval that we shall define below. As can be noted from Fig. 5, the period is a piecewise continuous, increasing function of $\overline{g}$. To explain this, we will show for the n–n solution that while the interspike interval between successive spikes of the free cell remains as T, the interval between the last (n th) spike of the free cell and the first spike of the other cell is less than or equal to T. As $\overline{g}$ increases, this interval increases to T at which point the n–n solution bifurcates. We will then show that this bifurcation point occurs when the period is $2nT$.

Let us return again to the 1–1 firing pattern. Assume that at $t=0$, cell 1 becomes free and jumps to the active state with an initial value of d_1 given by $d_1(0)$. Cell 1 returns to the silent state at $t=T_{act}$ with $d(T_{act}) = d_1(0)\exp(-T_{act}/\tau_b)$. Now cell 2 will become free at some time $t = T_{act} + \Delta t$, where $\Delta t < T_{inact}$ needs to be determined. Cell 2 jumps to the active state staying there until $t = \Delta t + 2T_{act}$. Then at $t = 2(\Delta t + T_{act})$, cell 1 is ready to become free again. During the time $t \in (T_{act}, 2(\Delta t + T_{act}))$, d_1 increases according to $d' = (1-d)/\tau_a$. Thus at $t = 2(\Delta t + T_{act})$,

$$d_1(2(\Delta t + T_{act})) = 1-(1-d_1(T_{act}))e^{-(2\Delta t + T_{act})/\tau_a}.$$

Imposing the periodicity condition that $d_1(0) = d_1(2(\Delta t + T_{act}))$ implies that

$$d_{1-1}(\Delta t) = \frac{1-e^{-(2\Delta t + T_{act})/\tau_a}}{1-e^{-T_{act}/\tau_b}e^{-(2\Delta t + T_{act})/\tau_a}}. \quad (15)$$

Thus the value of d_{1-1} depends on Δt. This value Δt can be calculated for any initial value of the synaptic conductance $g_0 > g^\star$ by using the necessary and sufficient condition for firing $g < g^\star$. Thus we impose the firing condition $g(\Delta t) = g^\star$. Therefore, Δt satisfies

$$\Delta t(g_0) = \tau_k \ln \frac{g_0}{g^\star}. \quad (16)$$

The key point is to recognize that the periodic solution satisfies $g_0 = \overline{g}d_{1-1}(\Delta t)$. Thus to find the value of Δt for the 1–1 solution, define $q(\Delta t) = \tau_k \ln(\overline{g}d_{1-1}(\Delta t)/g^\star)$ and $r(\Delta t) = \Delta t$. The condition given in (16) is equivalent to finding an intersection of the graphs of $q(\Delta t)$ and $r(\Delta t)$ (Fig. 8). Let us now show that such an intersection exists and is unique for each value of $\overline{g}$. First consider $\Delta t = 0$. Then $q(0) = \tau_k \ln \overline{g}d_{1-1}(0)/g^\star$ where

$$d_{1-1}(0) = \frac{1-e^{-T_{act}/\tau_a}}{1-e^{-T_{act}/\tau_b}e^{-T_{act}/\tau_a}}.$$

Note that $0 < d_{1-1}(0) < 1$. We will require that $\overline{g}d_{1-1}(0) > g^\star$. Thus $q(0) > 0$. Observe that $r(0) = 0$. Therefore, $q(0) - r(0) > 0$. Next take the limit as $\Delta t \to \infty$. From (15), $d_{1-1}(\Delta t) \to 1$, and thus $q(\Delta t) \to \tau_k \ln \overline{g}/g^\star$ which is bounded from above. However, $r(\Delta t)$ is unbounded as $\Delta t \to \infty$. Thus for Δt sufficiently large, $q(\Delta t) - r(\Delta t) < 0$. Given the continuity of these two function, using the Intermediate Value Theorem, there exists a value $\Delta t^\star_{1-1} \in (0,\infty)$ such that $q(\Delta t^\star_{1-1}) = r(\Delta t^\star_{1-1})$ (Fig. 8).

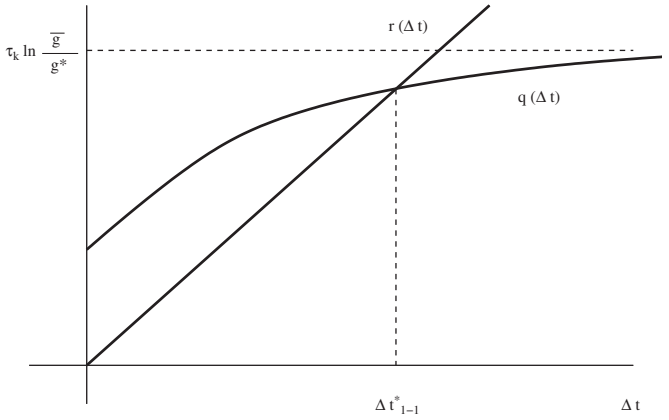

Fig. 8. The functions $q(\Delta t)$ and $r(\Delta t)$. Their point of intersection corresponds to the time between the end of a spike of one cell and the beginning of the spike of the other.

The uniqueness of $\Delta t^\star_{1-1}$ can be established through the following observations. First note that $dq(\Delta t)/d\Delta t > 0$ implying that $q(\Delta t)$ is an increasing function. Second, observe that

$$\frac{d^2q(\Delta t)}{d\Delta t^2} = \frac{-\tau_k}{d_{1-1}^2}\left(\frac{dd_{1-1}}{d\Delta t}\right)^2 + \tau_k \frac{d^2 d_{1-1}}{d\Delta t^2}.$$

The first term above is clearly negative. The second is as well since d_{1-1} is concave down with respect to Δt implying that its second derivative is negative. Thus $q(\Delta t)$ is an increasing concave down function. Since $q(0) > r(0)$, this implies that the intersection must be unique.

The value $\Delta t^\star_{1-1}$ is an increasing function of $\overline{g}$. Indeed $q(\Delta t)$ is an increasing function of $\overline{g}$ as it simply shifts up in the $q(\Delta t)$ versus Δt plane. This implies that the intersection with $r(\Delta t)$ shifts to the right to larger values of Δt with increasing $\overline{g}$.

A condition for 1–1 firing can now be stated in terms of $\Delta t^\star_{1-1}$. Namely, 1–1 firing is only possible if $\Delta t^\star_{1-1} < T_{inact}$ where the interspike interval separating the spikes of cell 1 and 2 is $T_{act} + \Delta t^\star_{1-1} \le T$. Once this condition is violated, the free cell spikes twice before the quiet cell can fire and thus the solution is no longer 1–1. Further, the condition also implies that a 1–1 solution bifurcates to another solution when $\Delta t^\star_{1-1} = T_{inact}$ and the period of the oscillation is exactly twice the intrinsic period, namely $2T$. This is consistent with numerical results shown in Table 1. Note that the condition in Eq. (5) continues to hold with $d_{1-1}(\Delta t^\star_{1-1})$ and T_{inact} replaced by $\Delta t^\star_{1-1}$. It is seen above how increases in $\overline{g}$ can make this condition impossible to hold, providing an upper bound on the terminal value of $\overline{g}$ (see Table 1) for which the 1–1 solution exists.

Let us now turn our attention to deriving necessary conditions for 2–2 firing patterns. In this case, starting at $t=0$ the free cell spikes twice. We define Δt to be the time from when the free cell ends the active state of its second spike to the time when the quiet cell escapes and fires. A necessary condition for the 2–2 solution to exist is that $\Delta t \le T_{inact}$. As before, we derive d_{2-2}, now as a function of Δt, and provide bounds to guarantee that the free cell spikes exactly twice. The value $d_{2-2}(\Delta t)$ satisfies

$$d_{2-2}(\Delta t) = \frac{1-(1-(1-e^{-T_{inact}/\tau_a})e^{-T_{act}/\tau_b})e^{-(T+2\Delta t+T_{act})/\tau_a}}{1-e^{-2T_{act}/\tau_b}e^{-(T+2\Delta t+T_{act})\tau_a}}. \quad (17)$$

For a particular fixed value of $\overline{g}$, we find the value $\Delta t^\star_{2-2}$ for which the periodic solution exists by using $g_0 = \overline{g}d_{2-2}(\Delta t)$ in our definition of the function $q(\Delta t)$. Thus the value $\Delta t^\star_{2-2}$ that satisfies the firing time condition for the 2–2 solution will differ from that of the 1–1 solution. Nonetheless, it is straightforward to show that it is an increasing

function of $\overline{g}$. The condition to ensure 2–2 firing now becomes

$$\overline{g}[1-(1-d_{2-2}(\Delta t^{\star}_{2-2})e^{-T_{act}/\tau_b})e^{-T_{inact}/\tau_a}]e^{-\Delta t^{\star}_{2-2}/\tau_k} < g^{\star} < \overline{g}d_{2-2}(\Delta t^{\star}_{2-2})e^{-T_{inact}/\tau_k}. \quad (18)$$

The first inequality guarantees that the free cell spikes no more than twice, while the latter guarantees that it spikes at least twice. When $\Delta t^{\star}_{2-2} = T_{inact}$ and the cycle period is $2(T+T_{act}+\Delta t^{\star}_{2-2}) = 4T$, the 2–2 solution bifurcates to a 3–3 solution. Clearly these ideas can be used to generalize the conditions for n–n firing which we leave to the interested reader.

Regarding co-existence of solutions, it remains straightforward to write down conditions for which this will occur. Namely, we still choose values of $\overline{g}$ that are small enough to guarantee n–n firing, but large enough to guarantee $(n+1)$-$(n+1)$ firing. For example, co-existence occurs between 1–1 and 2–2 firing when

$$\overline{g}d_{1-1}(\Delta t^{\star}_{1-1})e^{-\Delta t^{\star}_{1-1}/\tau_k} < g^{\star} < \overline{g}d_{2-2}(\Delta t^{\star}_{2-2})e^{-T_{inact}/\tau_k}. \quad (19)$$

Whether (19) is satisfied can be checked numerically for particular sets of parameters.

3.5. Heterogeneity in synaptic conductances

We now consider the case when there is heterogeneity in the synapses between cells and investigate the existence of n-m anti-phase solutions. In particular, we allow the maximal synaptic conductances between cells to differ by replacing $\overline{g}$ in (1) with $\overline{g}_{ji}$ which denotes the maximal conductance from cell j to cell i. It is straightforward to use the analysis of the previous sections to find different n-m solutions where cell 1 fires n times, followed by m spikes of cell 2.

Let us return for the sake of simplicity to the assumption that some cell spikes at every time nT. As an example, let us determine the conditions for a 2–1 solution in which cell 1 fires twice followed by cell 2 firing once. In this case, the period is $3T$. To guarantee that cell 1 spikes at least twice, we need $\overline{g}_{12}s_1(T^-) > g^{\star}$. That is, we need sufficient inhibition from cell 1 to be present to keep cell 2 from firing after one cycle. To guarantee that cell 1 spikes no more than twice, we require $\overline{g}_{12}s_1(2T^-) < g^{\star}$. Similarly, to guarantee that cell 2 spikes no more than once, we require $\overline{g}_{21}s_2(3T^-) < g^{\star}$. To find the values of $s_i(nT^-)$ we impose periodicity and find the relevant maximum values of d_i. Denote these as $d_{1,\max}$ and $d_{2,\max}$. Using Eq. (3), we find

$$d_{1,\max} = \frac{1-(1-(1-e^{-T_{inact}/\tau_a})e^{-T_{act}/\tau_b})e^{-(T+T_{inact})/\tau_a}}{1-e^{-2T_{act}/\tau_b}e^{-(T+2T_{inact})\tau_a}},$$

$$d_{2,\max} = \frac{1-e^{-(2T+T_{inact})/\tau_a}}{1-e^{-T_{act}/\tau_b}e^{-(2T+T_{inact})/\tau_a}}.$$

The necessary condition for 2-1 firing can then be stated as

$$\overline{g}_{21}d_{2,max}e^{-T_{inact}/\tau_k} < g^{\star} < \overline{g}_{12}d_{1,max}e^{-T_{inact}/\tau_k}. \quad (20)$$

In general, numerical simulations illustrate that it is reasonably straightforward how to choose $\overline{g}_{12}$ and $\overline{g}_{21}$ to create n–m firing patterns. The reason is that the control of when the quiet cell fires lies with the free cell. For example, in the Morris–Lecar network if $\overline{g}_{12}$ and $\overline{g}_{21}$ are initially chosen so that a solution lies in the 4-4 firing range, a decrease in $\overline{g}_{21}$ allows cell 1 to escape earlier from inhibition, before cell 2 fires a 4th spike. This creates a transition to 4–3 anti-phase firing. For progressively smaller values of $\overline{g}_{21}$, the solution transitions to 4–2 and 4–1 firing patterns (Fig. 9). Note, however, in Fig. 9 we had to also slightly increase $\overline{g}_{12}$ from 0.545 to 0.558 mS/cm^2 to obtain the 4–1 solution. Below we discuss reasons why this increase may be necessary.

We sampled the $\overline{g}_{12}-\overline{g}_{21}$ parameter space in numerical simulations of the Morris–Lecar network to create an n–m firing bifurcation diagram (Fig. 10). The labeled regions where different n–m anti-phase

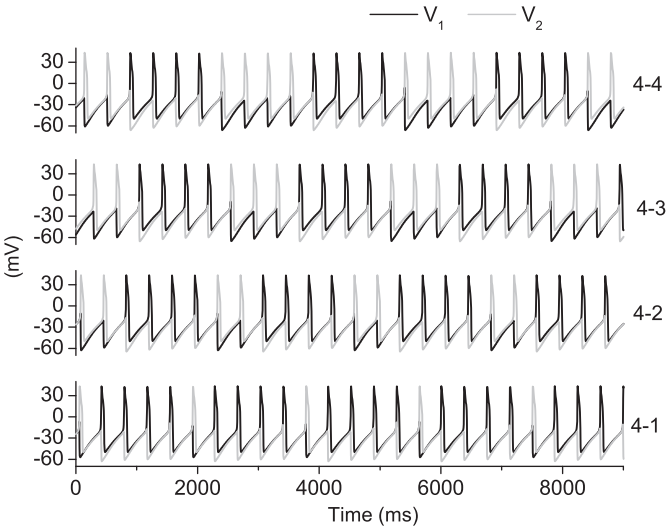

Fig. 9. Transitions between n–m antiphase solutions in the two-cell mutually inhibitory Morris–Lecar network as $\overline{g}_{12}$ and $\overline{g}_{21}$ are varied. When $\overline{g}_{12} = \overline{g}_{21} = 0.545$ mS/cm^2 (top panel), cell 1 (black) and cell 2 (gray) are in a numerically stable 4–4 antiphase solution. As $\overline{g}_{21}$ is decreased, cell 1 is less inhibited and firing patterns switch to 4–3 (2nd panel, $\overline{g}_{21} = 0.5$ mS/cm^2) and 4–2 (3rd panel, $\overline{g}_{21} = 0.4$ mS/cm^2) anti-phase solutions. Numerically stable 4–1 anti-phase firing (bottom panel) is obtained for low $\overline{g}_{21}$ (0.25 mS/cm^2) and a higher value of $\overline{g}_{12}$ (0.558 mS/cm^2).

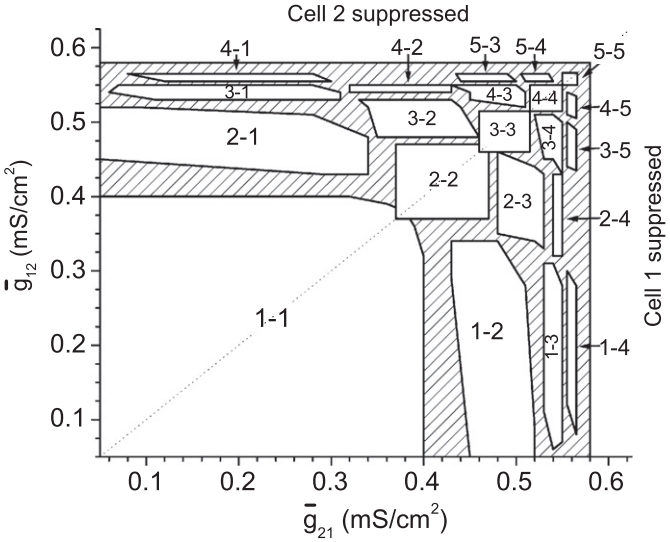

Fig. 10. Two-dimensional bifurcation diagram for numerically stable n–m anti-phase solutions (labeled regions) in the two-cell mutually inhibitory Morris–Lecar network as $\overline{g}_{12}$ and $\overline{g}_{21}$ are varied. In the hatched areas, solutions displayed more complicated, higher order dynamics. Small regions of co-existence between n–n solutions remained with heterogeneous values of $\overline{g}_{12}$ and $\overline{g}_{21}$.

solutions are numerically stable fall in regions of parameter space suggested by our analysis above. However, the diagram indicates a complexity of solutions that arise when synaptic strengths are heterogeneous. For example, the n–m solution regions do not exactly align with the n–n regions. Instead, there is a tendency for the regions to be located upwards or rightwards from the n–n regions as $\overline{g}_{21}$ or $\overline{g}_{12}$, respectively, is decreased from the diagonal. Additionally, in the unusually shaped hatched regions between numerically stable n–m regions, the solution did not settle into a simple n–m pattern. Instead, the solution displayed more complicated higher order dynamics. For example, at a point in the region between numerically stable 1–1 and 2–1 firing ($\overline{g}_{12} = 0.42, \overline{g}_{21} = 0.3$), there exists a periodic firing pattern that can be described as 2:1:1:1, in which cell one fires two spikes, cell

two fires one spike, cell one spikes once and then cell two spikes once to complete the repeating pattern. The complexity of solutions and the irregularity of parameter regions for numerically stable *n*-*m* firing results from changes in the period of a firing pattern on the depression variables that then influence the conditions for existence of the firing pattern. As an example, consider the 2–1 numerically stable firing region with a fixed value of $\overline{g}_{12}$ and decreasing $\overline{g}_{21}$. For numerically stable 2–1 firing, $\overline{g}_{21} < \overline{g}_{12}$ and the reduced inhibition from cell 2 to cell 1 allows cell 1 to escape from inhibition early. As $\overline{g}_{21}$ decreases, the time between the last cell 1 spike in a cycle and the first cell 1 spike of the next cycle is reduced. It is in this interval that the cell 1 synapse recovers from depression, thus as $\overline{g}_{21}$ decreases, the maximum value of the cell 1 depression variable, $d_{1,\max}$, also decreases. So, the right-hand inequality of Eq. (20) becomes harder to satisfy and may require an increase in $\overline{g}_{12}$ to remain satisfied. This interaction of changes in maximum synaptic conductance, cycle period, and synaptic depression and recovery between the cells restricts the possible combinations of parameters that can satisfy our conditions for existence of *n*--*m* patterns.

Another effect of changes in cycle period of an *n*-*m* firing pattern, that is not accounted for by our analysis but may contribute to the complexity of solutions, is that the effect of synaptic input can depend on the timing of the input relative to the cell's oscillation. For weakly coupled systems, this effect can be summarized in a phase response curve for an oscillator which tracks the change in timing of firing of a subsequent spike if the oscillator is perturbed at different phases of its cycle. But for strongly coupled systems, such as the one we are considering, the oscillator receiving the inhibition is far away in phase space from its intrinsic trajectory. Thus PRC analysis is not directly applicable. Nonetheless, we note that for our cell modeled with the Morris–Lecar equations, an inhibitory input delays the firing of a subsequent spike if the input arrives in the later half of the cell's cycle, and the amplitude of the delay increases as the timing of the input approaches the time of firing of the subsequent spike. For numerically stable 2–1 firing with a fixed value of $\overline{g}_{12}$ and decreasing $\overline{g}_{21}$, for example, as cell 1 escapes from inhibition earlier relative to the free trajectory of cell 2, the effect of the inhibition on delaying cell 2 firing decreases. However, as further discussed in the next section, it is not straightforward to predict how this decrease in delay of firing affects our conditions for 2–1 firing. But we can certainly see that the conditions will be influenced. For example, continuing with the case of 2–1 firing, phase-dependent variations in effects of inhibition will affect the timing of the first firing of the quiet cell such that it is not at nT. Our analysis in Section 3.4 indicates that $d_{i,max}$ depends on this interspike interval. Thus, in the necessary condition for 2–1 firing (Eq. (20)), variation in $\overline{g}_{ji}$ will induce variations in $d_{i,\max}$ and $d_{j,\max}$ to modify the $\overline{g}_{12}-\overline{g}_{21}$ parameter region where 2–1 firing is possible.

4. Discussion

Networks of inhibitory neurons arise throughout the nervous system, either in isolation or as part of larger excitatory-inhibitory networks. Much attention has been devoted to understanding the circumstances under which inhibition leads to synchronous (Van Vreeswijk et al., 1994) or out-of-phase behaviour (Bem and Rinzel, 2004; Skinner et al., 1994). Some studies have emphasized that the pattern of activity of inhibitory sub-networks often plays an important role in determining the global dynamics of the full network (Terman et al., 2002). Anti-phase rhythmic firing patterns are a common feature of many systems. For example, in central pattern generators, i.e. networks in which oscillations exist in the absence of sensory input, anti-phase patterns can arise through the interaction of pairs or groups of mutually inhibitory neurons (Marder and Calabrese, 1996; Nadim et al., 1998). Establishing proper phase relationships between neurons in anti-phase, or, more generally, in out-of phase patterns is often critical for motor control of rhythmic movements (Hooper, 1996; Williams and Sigvardt, 1992). Thus theoretical and modeling studies involving networks of mutually coupled inhibitory neurons can shed light on the neural mechanisms that underlie many of these behaviors.

Given that the nervous system is comprised of a finite, albeit large, number of neurons, it is of value for a given network to be able to contribute to multiple tasks. Multistability of solutions provides an efficient and elegant way for a particular network to achieve this. Multistability in neuronal rhythms has been suggested to have functional relevance for many different tasks such as working memory (Brunel, 2003) (also see review in Constantinidis and Wang, 2004), in the limbic system for control of head direction in rats (Zhang, 1996) and in the initiation of cortical seizures (Takeshita et al., 2007), to name only a few examples. Skinner et al. (2005) have studied how multistability in networks consisting of just two neurons can relate to different types of activity patterns in larger networks. Other studies have investigated mechanisms that give rise to multistable behavior. For example, Foss and Milton (2000) showed how synaptic delay can initiate mutistability in Aplysia motoneurons. Matveev et al. (2007) showed how the existence of low-threshold calcium-mediated *T*-type currents can instigate multistable bursting patterns in a model of mutually coupled neurons.

In this paper, we have shown that in a relatively simple network of two oscillatory neurons mutually coupled through inhibition, synaptic depression introduces a multitude of numerically stable anti-phase firing patterns and promotes co-existence between them. Moreover, the type of pattern that exists can largely be predicted by knowing the strengths of the maximal conductances of the two synapses. Namely, the cell that projects a stronger synapse dominates firing in the anti-phase pattern and the extent of domination is graded as synaptic strength is varied. Our work is closely related, but complementary to that of Jalil et al. (2004) who studied how synaptic depression invoked different bursting patterns in a model of two mutually coupled hippocampal basket cells. They showed through a series of simulations how novel patterns arise as the degree of heterogeneity in depression time constants is varied. In particular, they describe a set of solutions called alternating bursting (AB) solutions which are analogous to our *n*–*m* solutions in which the cells alternate bursts of different numbers of spikes. They used the slightly more complicated Tsodyks and Markram model (Tsodyks and Markram, 1997) for depression than the one we use here. However, the qualitative features of the two depression models are similar. They also used the more complicated interneuron model of White et al. (1998) to describe their intrinsic oscillators. Perhaps due to these reasons, Jalil et al. focused on giving an intuitive explanation for the existence of various patterns without providing a mathematical analysis. Our paper, to some degree, provides the mathematical basis for their results, by beginning to derive the generic conditions that must be met to obtain co-existence in networks of inhibitory neurons coupled by depressing synapses. While we did not explicitly mimic their study of AB solutions by changing the depression time constant, our conditions on co-existence with heterogeneity, given in Eq. (20) for example, can easily be recast in terms of the depression time constants to provide analytic bounds for when the AB pattern should exist.

In Manor and Nadim (2001), Manor and Nadim experimentally considered, through a dynamic clamp-mediated hybrid circuit, a network of two inhibitory cells, reciprocally coupled by two depressing synapses where the biological cell was a bursting pacemaker and the model cell was non-oscillatory. They showed that this network robustly displayed bistability of a cell-controlled

and a synapse-controlled anti-phase firing pattern. In the cell-controlled case, both depressing synapses were weak and the intrinsic properties of the pacemaker neuron governed the oscillatory solution. In the synapse-controlled case, both synapses were able to recover from depression during the oscillatory cycle and these synaptic dynamics controlled the oscillation. In the context of the current paper, weak can be interpreted as a small value of d_{1-1} while strong means a large value of d_{1-1}. Similarly, in Bose et al. (2001), we showed bistability in an excitatory-inhibitory two cell network between in-phase oscillations of high frequency (cell-controlled) and of low frequency (synapse-controlled). These results establish that depression allows the synapse to operate in two distinct stable patterns, leading to two distinct solutions. In the current paper, we have found n–n solutions for $n \geq 1$ that are all synapse-controlled patterns, since release from inhibition of the quiet cell is governed by synaptic dynamics. It is interesting to note that our analysis shows how there are different gradations of the synaptic strength that give rise to different solutions. Instead of there being a single synapse-controlled solution, there is now a family of synapse-controlled solutions. The ability of depression to allow the synapse to operate at distinct steady states contributes to the co-existence of different synapse-controlled modes. Further the analysis shows how the intrinsic properties of the neurons take on a diminished role in these synapse-controlled rhythms. Thus our results are quite general in that they imply that for many neuronal models of a spiking neuron, a parameter regime can be found whereby a network of cells coupled by depressing inhibitory synapses will display synapse-controlled multistabilty of the form described in this paper. Undoubtedly, the neuron model in question would need to satisfy certain assumptions which would involve how the neuron responds to inhibitory inputs (e.g. that the neuron return quickly to its intrinsic limit cycle after inhibtion). Jalil et al. (2004) do consider the question of multistability. However, the type of multistability considered is between alternating bursting and other patterns such as synchronous firing, or results directly from the existence of multistability in the non-depressed network. We suspect that multistability of alternating burst solutions in their model should also exist. To be clear, however, our results by no means exhaustively categorize all situations which lead to multistability. Even when the conditions we identify here are not met, such as the free cell spiking with its intrinsic period T, multistability is still possible (Matveev et al., 2007).

While we have discussed the co-existence of anti-phase solutions, we have not mentioned either the existence or possible co-existence of synchronous solutions, ones in which the two cells behave identically in time. Prior studies have shown that when the decay rate of the inhibition is sufficiently small, then it is possible for inhibition to synchronize cells (Terman et al., 1998; Van Vreeswijk et al., 1994). These studies showed, however, that either an explicit delay to the onset of the inhibition or a sufficiently slow rise time of the inhibitory synapse is a necessary condition for synchronization. In our study, we use a parameter regime that corresponds to slowly decaying inhibition, but also one in which there is zero rise time to the onset of inhibition. Thus while a synchronous solution may co-exist with an anti-phase solution, it is unstable and we would not expect to observe it.

A major simplification that we pursued in our analysis of these anti-phase solutions was to derive conditions for the existence of solutions as opposed to actually proving existence of these solutions. In order to actually prove existence, a typical way to proceed in these types of problems is to define an identifiable event (such as the time when a cell fires, or the time when it returns to the silent state). One then measures all unknown variables every time this event occurs, thereby defining a type of return map. If the map can be defined to be much lower in dimension than the original system, then an advantage is gained in terms of analysis. In the present context, the separation of time scales and the coupling of s to d at the moment a cell jumps to the active state suggests that the identifiable event should be the moment when either cell jumps to the active state. Doing so and further assuming that the active duration of a cell is short compared to the inactive duration would allow us to define a four-dimensional map that measures (w_1, s_1, w_2, s_2) at each iterate. A fixed point of this map would correspond to a 1–1 or suppressed solution, a period 2 point to a 2–2 solution and so on. This map can effectively be reduced to a two-dimensional map if we assume that the exact (w_i, s_j) value of free cell i at the moment of the jump is irrelevant allowing us to simply measure the values w_j of the quiet cell and s_i. By assuming that the function $h(v,w)$ in Eq. (1) is large relative to the synaptic decay rate when a cell is silent, we can further reduce the two-dimensional map to consider just the s value at the moment a cell jumps to the active state. This, in fact, is what gave rise to our necessary and sufficient condition for firing in Section 3.4 and is a natural consequence of being in a synapse-controlled parameter regime. Stability of solutions can then be determined by linearizing at a fixed point of the map (or its composition) and estimating the ensuing eigenvalues. By deriving and analyzing a lower-dimensional map, there is also a chance of understanding the nature of the bifurcation that occurs between different firing patterns. For example, the map may be helpful in determining why there are unstable branches extending from the numerically stable branches that form isolas shown for the 1–1, 2–2, 3–3 and suppressed solutions in Fig. 5. The reduction to lower dimensional set of necessary conditions that we have performed also leaves unexplained why the regions for n–m firing in Fig. 10 are so oddly shaped. Near the boundaries of these regions the simple one-dimensional conditions analogous to Eq. (20) are not sufficient to guarantee the existence of a periodic solution. Presumably the assumptions that we made that ignored the specific values of the w_i recovery variables of the two neurons no longer hold and there the dynamics can only be captured by a higher dimensional approximation. It remains an open question that we continue to pursue as to what other conditions need to be enforced there to obtain solutions.

A natural question to consider is whether the current methods extend to study activity patterns in a three-cell or larger inhibitory network. Typical solutions that one finds in such networks are clustered activity patterns where the cells break up into distinct groups consisting of a number of cells synchronized with one another but oscillating out-of-phase with other groups (Golomb and Rinzel, 1994). We have previously studied a globally inhibitory network with synapses that display depression and showed how multistability of cluster solutions can arise (Chandrasekaran et al., 2009). These solutions consisted of single spikes per cluster similar to our 1–1 solutions and were obtained through analyzing an n-dimensional map. There we had to keep track of not just the level of depression in the system, but also the values of recovery variables (equivalent to w in our case). Thus in a larger network, if we wished to find clustered solutions in which the cells fired several spikes per cycle, like our n–n solutions, at a minimum we would need to study a much higher dimensional set of conditions. There is nothing precluding the pursuit of lower dimensional necessary conditions as we have done here. However, the range of interesting patterns that one would find by reducing all the way down to a one-dimensional set of necessary conditions would be rather small.

Our results concerning the co-existence of n–m solutions touched on the issue of how phase relationships between cells may affect not only the existence of periodic solutions, but also our ability to predict their existence. In general, the manner in which a neuron responds to weak inputs can be categorized through its phase response curve (PRC), which measures the change in phase of an oscillator to inputs arriving at different phases of the cycle. PRCs

have been used in many situations to understand phase-locking in networks of neurons (see Canavier and Achuthan, 2010 for a recent review). The main issue that prevents their direct application here regards the strength of the coupling. The theoretical framework underlying PRC analysis is one of weak coupling between neurons. In our case, the coupling between neurons, while depressing, is not weak. As a result, the quiet cell in our models is placed in a different location in phase space, due to the synaptic inhibition, than its intrinsic oscillatory trajectory from where the PRC was originally computed.

Although we are not able to directly use PRC analysis, it is still valid to ask what phase relationship exists between the two neurons in any of the n–n solutions. For 1–1 solutions, this question is easily answered, namely, the cells are in anti-phase, with each cell firing at exactly phase 0.5. We note that as $\bar{g}$ increases in the 1–1 regime, the period of the oscillations will change, but the phase of firing is constant. This is because $T_{act}+\Delta t^{\star}_{1-1}$ that measures the time of firing of cell 2 after cell 1 fires is the same as the time of firing of cell 1 after cell 2 fires and this is exactly half the period of the coupled system. For the same reason, in an n–n solution, the phase at which the quiet cell will fire relative to the cycle period of the coupled system $2(nT+T_{act}+\Delta t^{\star}_{n-n})$ is also 0.5. The firing phases of each of the other $2n-1$ spikes within the cycle can be calculated since these spike times are known.

Calculating the phase of firing of cells within an n–m solution can easily be done under the assumption that some cell fires every multiple of the intrinsic period T. In this case, if cell 1 fires n spikes and cell 2 fires m spikes, then the phase of the first spike of cell 2 relative to the cycle period $(n+m)T$ is simply $n/(n+m)$. The phase of the first spike relative to the intrinsic period of the oscillator T is simply 0.5. The difficulty arises in determining phase when the condition of firing every multiple of T is relaxed. In this case, there is no obvious way from the one-dimensional quantities we have been using to calculate the time difference from the last spike of cell 1 to the first spike of cell 2 and vice versa. Moreover, unlike in the homogenous case, there is no reason why these two times should be the same. Here a higher dimensional approximation of the neuronal network is needed to address the question of phase.

In summary, the mathematical analysis presented in this paper represents the middle ground between rigorously proving the existence and stability of solutions and relying solely on numerical simulations. This trade-off has allowed us to extract the important features of the model, and in particular of synaptic depression, that tend to dominate and dictate the interesting dynamics displayed by the network. We believe that similar approaches can be used to shed light on the dynamics of more complicated neuronal networks especially ones in which short-term synaptic plasticity plays a critical role in organizing the network dynamics.

Acknowledgements

This work was supported in part by grants from the National Science Foundation DMS-0315862 (AB, VB), DMS-0615168 (AB), DBI-0340687 (VB) and the United States India Educational Foundation under the Fulbright-Nehru Program (AB).

Appendix A

For the Hodgkin–Huxley model network, the function $f(v_i, w_i)$ in (1) contains terms describing an inward sodium current, an outward potassium current, a linear leak current and an external applied current, and the variable w_i is a three-dimensional vector containing the gating variables $m_i(t)$, $q_i(t)$ and $n_i(t)$:

$$v_i' = -g_{Na}m_i^3 q_i(v_i-E_{Na})-g_K n_i^4(v_i-E_K)-g_l(v_i-E_l)+I_{app}-\bar{g}s_j(v-E_{inh}),$$

where i, $j=1$, 2. The vector function $h(v_i,\vec{w}_i)$ models the activation and inactivation kinetics of the sodium and potassium conductances:

$$x_i' = \alpha_x(v_i)(1-x_i)-\beta_x(v_i)x_i,$$

where $x = m$, q or n. The rate functions for the gating variables are

$$\alpha_m(v_i) = -0.1(v_i+40)/(\exp(-(v_i+40)/10)-1)$$
$$\beta_m(v_i) = 4\exp(-(v_i+65)/18),$$

$$\alpha_q(v_i) = 0.07\exp(-(v_i+65)/20)$$
$$\beta_q(v_i) = 1.0/(\exp(-(v_i+35)/10)+1),$$

$$\alpha_n(v_i) = -0.01(v_i+55)/(\exp(-(v_i+55)/10)-1)$$
$$\beta_n(v_i) = 0.125\exp(-(v_i+65)/80).$$

Maximum conductance values are $g_{Na}=120$, $g_K=36$ and $g_l=0.3$ mS/cm^2. Reversal potentials are $E_{Na}=50$, $E_K=-77$, $E_l=-54.4$ and $E_{inh}=-80$ mV. Applied current was set to $I_{app}=7$ μA/cm^2.

For the Morris–Lecar model network, the function $f(v_i,w_i)$ in (1) contains an inward calcium current, an outward potassium current, a linear leak current and an external applied current:

$$v_i' = -g_{Ca}m_\infty(v_i)(v_i-E_{Ca})-g_K w_i(v_i-E_K)-g_l(v_i-E_l)+I_{app}-\bar{g}s_j(v-E_{inh}),$$

where i, $j=1$, 2. The function $h(v_i,w_i)$ models the kinetics of the potassium conductance:

$$w_i' = \frac{w_\infty(v_i)-w_i}{\tau_w},$$

with time constant $\tau_w=100$ ms. Steady state activation functions for the calcium and potassium conductances are $m_\infty(v)=(1+\tanh((v-v_a)/v_b)/2$ and $w_\infty(v)=(1+\tanh((v-v_c)/v_d)/2$ where $v_a=1$, $v_b=14.5$, $v_c=4$ and $v_d=15$ mV. Maximum conductance values are $g_{Ca}=0.3$, $g_K=0.6$ and $g_l=0.15$ mS/cm^2. Reversal potentials are $E_{Ca}=100$, $E_K=-70$, $E_l=-50$ and $E_{inh}=-80$ mV. Applied current was set to $I_{app}=3.8$ μA/cm^2.

In both networks, dynamics of the synaptic gating s_i and its depression variable d_i ($i=1,2$) were governed by

$$s_i' = \frac{-s_i}{\tau_\kappa}H_{down}(v_i)+\frac{d_i-s_i}{\tau_\gamma}H_{up}(v_i),$$

$$d_i' = \frac{1-d_i}{\tau_a}H_{down}(v_i)-\frac{d_i}{\tau_b}H_{up}(v_i), \qquad (21)$$

where $H_{down}(v)=1/(1+\exp((v-v_\theta)/k_\theta))$ and $H_{up}(v)=1/(1+\exp(-(v-v_\theta)/k_\theta))$ with the slope of these continuous Heaviside functions set to $k_\theta=0.1$ mV. The synaptic threshold was set to $v_\theta=0$ mV for the Morris–Lecar network and $v_\theta=-10$ mV for the Hodgkin–Huxley network. Time constants for the synaptic conductances and depression variables in the Hodgkin–Huxley network are $\tau_\kappa=4$, $\tau_\gamma=1\times10^{-4}$, $\tau_a=47$ and $\tau_b=4$ ms. For the Morris–Lecar network, the synaptic parameters are $\tau_\kappa=100$, $\tau_\gamma=1\times10^{-4}$, $\tau_a=1000$ and $\tau_b=100$ ms. For simulations with non-depressing synapses, d_i in the second term of the right-hand side of Eq. (21) is replaced by 1 and other parameters remain the same for each network. Values of the maximum synaptic conductances $\bar{g}$ when the synapses are identical, and $\bar{g}_{12}$, $\bar{g}_{21}$ when heterogeneous synapses are considered, are given in the text and figure captions. Note the equation for s_i is slightly different than what is shown in (1). For the numerical simulations, we have smoothed out the reset of s_i to d_i at the moment a presynaptic cell goes above threshold. We have also allowed $s_i=d_i$ throughout the entire active state of the presynaptic neuron. These changes were made to facilitate numerical computation of bifurcation diagrams (Figs. 5 and 10) using AUTO via the interface provided by XPPAUT

(Ermentrout, 2002). Numerical simulations of network models were computed using an adaptive step-size integrator for stiff differential equations implemented with XPPAUT.

References

Abbott, L., Regehr, W., 2004. Synaptic computation. Nature 431, 796–803.

Abbott, L.F., Varela, J.A., Sen, K., Nelson, S.B., 1997. Synaptic depression and cortical gain control. Science 275, 220–224.

Barbieri, F., Brunel, N., 2007. Irregular persistent activity induced by synaptic excitatory feedback. Front. Comput. Neurosci. 1, 5.

Bem, T., Rinzel, J., 2004. Short duty cycle destabilizes a half-center oscillator, but gap junctions can restabilize the anti-phase pattern. J. Neurophysiol. 91, 693–703.

Bose, A., Manor, Y., Nadim, F., 2001. Bistable oscillations arising from synaptic depression. SIAM J. Appl. Math. 62, 706–727.

Brunel, N., 2003. Dynamics plasticity of stimulus-selective persistent activity in cortical network models. Cereb. Cort. 13, 1151–1161.

Canavier, C., Achuthan, S., 2010. Pulse coupled oscillators and the phase resetting curve. Math. Biosci. 226, 77–96.

Chandrasekaran, L., Matveev, V., Bose, A., 2009. Multistability of clustered states in a globally inhibitory network. Physica D 238, 253–263.

Constantinidis, C., Wang, X.-J., 2004. A neural circuit basis for spatial working memory. Neuroscientist 10, 553–565.

Ermentrout, G.B., 2002. Simulating, Analyzing, and Animating Dynamical Systems: A Guide to XPPAUT for Researchers and Students. SIAM, Philadelphia, PA.

Foss, J., Milton, J., 2000. Multistability in recurrent loops arising from delay. J. Neurophysiol. 84, 975–985.

Golomb, D., Rinzel, J., 1994. Clustering in globally inhibitory neurons. Physica D 72, 259–282.

Grande, L., Spain, W., 2005. Synaptic depression as a timing device. Physiology 20, 201–210.

Hodgkin, A., Huxley, A., 1952. A quantitative description of membrane current and its application to conduction and excitation in nerve. J. Physiol. 117, 500–544.

Hooper, S., 1996. Phase maintenance in they pyloric pattern of the lobster (*Panulirus interruptus*) stomatogastric ganglion. J. Comput. Neurosci. 4, 191–205.

Jalil, S., Grigull, J., Skinner, F., 2004. Novel bursting patterns emerging from model inhibitory networks with synaptic depression. J. Comput. Neurosci. 17, 31–45.

Marder, E., Calabrese, R., 1996. Principles of rhythmic motor pattern generation. Physiol. Rev. 76, 687–717.

Manor, Y., Nadim, F., 2001. Synaptic depression mediates bistability in neuronal networks with recurrent inhibitory connectivity. J. Neurosci. 21, 9460–9470.

Manor, Y., Bose, A., Booth, V., Nadim, F., 2003. The contribution of synaptic depression to phase maintenance in a model rhythmic network. J. Neurophysiol. 90, 3513–3528.

Matveev, V., Bose, A., Nadim, F., 2007. Capturing the bursting dynamics of a two-cell inhibitory network using a one-dimensional map. J. Comput. Neurosci. 23, 169–187.

Mishchenko, M., Rozov, N., 1980. Differential Equations with a Small Parameter and Relaxation Oscillations. Plenum, New York.

Morris, C., Lecar, H., 1981. Voltage oscillations in the barnacle giant muscle fiber. Biophys. J. 35, 193–213.

Mouser, C., Nadim, F., Bose, A., 2008. Maintaining phase of the crustacean tri-phasic pyloric rhythm. J. Math. Biol. 57, 161–181.

Nadim, F., Manor, Y., Kopell, N., Marder, E., 1999. Synaptic depression creates a switch that controls the frequency of an oscillatory circuit. Proc. Natl. Acad. Sci. USA 96, 8206–8211.

Nadim, F., Manor, Y., Nusbaum, M., Marder, E., 1998. Frequency regulation of a slow rhythm by a fast periodic input. J. Neurosci. 18, 5053–5067.

O'Donovan, M.J., Wenner, P., Chub, N., Tabak, J., Rinzel, J., 1998. Mechanisms of spontaneous activity in the developing spinal cord and their relevance to locomotion. Ann. NY Acad. Sci. 860, 130–141.

Rabbah, P., Nadim, F., 2007. Distinct synaptic dynamics of heterogeneous pacemaker neurons in an oscillatory network. J. Neurophysiol. 97, 2239–2253.

Rubin, J.E., Hayes, J.A., Mendenhall, J.L., Del Negro, C.A., 2009. Calcium-activated nonspecific cation current and synaptic depression promote network-dependent burst oscillations. Proc. Natl. Acad. Sci. USA 106, 2939–2944.

Skinner, F., Kopell, N., Marder, E., 1994. Mechanisms for oscillation and frequency control in networks of mutually inhibitory relaxation oscillators. J. Comput. Neurosci. 1, 69–87.

Skinner, F., Bassazi, H., Campbel, S., 2005. Two-cell to N-cell heterogeneous, inhibitory networks: precise linking of multistable and coherent properties. J. Comput. Neurosci. 18, 343–352.

Tabak, J., Senn, W., O'Donovan, M., Rinzel, J., 2000. Modeling of spontaneous activity in developing spinal cord using activity-dependent depression in an excitatory network. J. Neurosci. 20, 3041–3056.

Takeshita, D., Sato, Y., Bahar, S., 2007. Transitions between multistable states as a model of epileptic seizure dynamics. Phys. Rev. E 75, 051925.

Terman, D., Kopell, N., Bose, A., 1998. The dynamics of two mutually coupled slow inhibitory neurons. Physica D 117, 241–275.

Terman, D., Rubin, J., Yew, A., Wilson, C., 2002. Activity patterns in a model for the subthalamodallidal network of the basal ganglia. J. Neurosci. 22, 2963–2976.

Tsodyks, M., Markram, H., 1997. The neural code between neocortical pyramidal neurons depends on the transmitter release probability. Proc. Natl. Acad. Sci. 94, 719–723.

Van Vreeswijk, C., Abbott, L., Ermentrout, B., 1994. When inhibition not excitation synchronizes coupled neurons. J. Comput. Neurosci. 1, 303–313.

White, J., Chow, C., Ritt, J., Soto-Trevino, C., Kopell, N., 1998. Synchronization and oscillatory dynamics in heterogeneous, mutually inhibited neurons. J. Comput. Neurosci. 5, 5–16.

Williams, T., Sigvardt, K., 1992. How the lamprey swims. Physiology 7, 161–165.

Zhang, K., 1996. Representation of spatial orientation by the intrinsic dynamics of the head-direction cell ensemble: a theory. J. Neurosci. 16, 2112–2126.